

Enhancement of the Anticorrosion Properties of Epoxy Resin Composites through Incorporating Hydroxylated and Silanised Hexagonal Boron Nitride (h-BN)

Jiansan Li*, Xiangqi Huang*, Jinye Bi

School of Mechanical and Automotive Engineering, South China University of Technology, Guangzhou 510640, PR China

*E-mail: jsli@scut.edu.cn (J.L.); 201921003345@mail.scut.edu.cn (X.H.)

Received: 13 October 2021 / Accepted: 22 November 2021 / Published: 2 February 2022

Hexagonal boron nitride (h-BN) has the outstanding properties of high-temperature stability, electrical insulation and impermeability against water, oxygen and corrosive ions. However, BN easily agglomerated in the coating, resulting in coating microporous defects and reducing the anticorrosive properties. Thus, h-BN was modified through a two-step treatment, hydroxylation and silanisation. h-BN modified by silane coupling agent 3-glycidoxypropyltrimethoxysilane (KH560) was characterized by Fourier transform infrared spectroscopy (FTIR), X-ray photoelectron spectroscopy (XPS) and scanning electron microscopy (SEM). Then, the corrosion resistance of the BN-KH/epoxy resin coatings was measured by electrochemical testing. The results demonstrated that the corrosion current density of the coating with modified h-BN nanosheets was decreased from $2.67 \times 10^{-7} \text{ A} \cdot \text{cm}^{-2}$ to $5.28 \times 10^{-8} \text{ A} \cdot \text{cm}^{-2}$ compared with that of the pure epoxy resin. The impedance of the composite coating with modified h-BN is $5.27 \times 10^7 \Omega \cdot \text{cm}^2$, approximately 20 times higher than that of the coating with the original h-BN ($1.95 \times 10^6 \Omega \cdot \text{cm}^2$) and the EP coating ($4.26 \times 10^5 \Omega \cdot \text{cm}^2$), indicating that BN-KH can protect the coating from damaging corrosive ions and that BN-KH/EP can maintain an excellent anticorrosion property.

Keywords: hexagonal boron nitride; corrosion resistance; modified; electrochemical impedance spectroscopy

1. INTRODUCTION

Epoxy resin is widely applied in anticorrosion fields due to its excellent bonding strength and chemical resistance. However, microporous defects easily form in the coatings because of operator negligence and solvent evaporation during the coating stage. This results in water, oxygen molecules and corrosive ions still easily passing through the coating and reaching the substrate to initiate or even accelerate corrosion of the metal, which reduces the anticorrosion properties of the coatings. Previous studies[1-2] have reported that adding materials with 2D lamellar structures to organic coatings will

increase the passage length of corrosive ions, and thus provide a physical barrier against the diffusion and penetration of the molecules, which is referred to as “the maze effect”[3].

In the recent surge in 2D material research, hexagonal boron nitride(h-BN) has attracted much attention owing to its outstanding properties of high-temperature stability[4], mechanics[5-7], electrical insulation and impermeability against water, oxygen[8] and corrosive ions[9-11]. h-BN is a species isoelectronic with graphene that shares similar physical and chemical properties and the lattice mismatch with graphene is only 1.7%[12]. As h-BN is white, it is also called “white graphene” [13]. Each layer of h-BN is composed of continuously extending hexagonal crystal planes, that consists of alternating sp^2 conjugated B and N atoms, while the vertical layers are stacked by van der Waals forces. Compared with the C-C bond of graphene, the partially polarized B-N bonds exhibits a certain ionic activity[8, 14]. In addition, the most significant difference between these two is that h-BN have high permittivity, which avoids the case in which materials with relatively high potential become cathodes compared with protected metal. In contrast, conducting graphene coatings can further promote corrosion by facilitating electrochemical reactions on the interface between the coating and substrate[15].

h-BN, with a perfect sp^2 honeycomb structure, large diameter-to-thickness ratio and dielectric properties, shows great potential in corrosion protection, whereas prior studies have paid particular attention to the thermal conductivity enhancement[16-19] of h-BN. However, a limited number of studies have been conducted to determine the anticorrosion effect of h-BN [20]. Shen et al.[21]revealed that the potential barrier for O_2 to pass through BN is close to that of graphene by density functional theory calculations. In their experiment, the h-BN monoatomic layer showed excellent long-term barrier properties, and due to the good dielectric properties of h-BN, galvanic corrosion was prevented. It was found that the Cl^- ions content and corrosion pits were significantly reduced after immersion in a simulated seawater medium for 30 days when the metal was coated with a h-BN/polymer coating, owing to its excellent chemical inertness, and hydrophobic, dielectric and barrier properties[22]. However, when BN powder is added as a filler to the coating, BN easily agglomerates in the coating because of its poor dispersibility and resin compatibility. This results in microporous defects with a reduction in the physical and chemical properties of the anticorrosive coating, which limits the application of BN in anticorrosion coatings. For this reason, BN is generally modified first before application.

Li et al.[23]treated BN with NaOH at high temperature to achieve hydroxylation of BN to improve the dispersion of BNNSs (BN Nanosheets) in water-borne polyurethane (WBE). The impedance of the coating doped with modified BN was 1-2 orders of magnitude higher than that of the pure PU coating. Wu et al.[24] selected hydrophilic GO as an intercalator to exfoliated h-BN and enhance its dispersion in WBE. The π - π interaction between GO and h-BN causes h-BN to be uniformly distributed on the surface of GO. In the electrochemical performance test, the composite coating with modified BN showed a higher modulus of impedance. Huang[25] used GO as the intercalating agent for BN with reduction of GO to rGO. After that PDA was grafted onto the surface of h-BN-rGO, which benefited the uniform distribution of this nanohybrid in the PVB coating. The best anticorrosion performance of the PVB composite coating with the nanohybrid filler is 2 orders of magnitude higher than that of pure PVB. Zhang et al.[26] provided a facile and environmental-friendly method for preparing the h-BN/PDA-KH560 nanohybrid. They considered that high impedance of the composite coating was related to the

layered structure, excellent performance in plugging micropores and the uniform dispersion of the nanohybrids in epoxy resin.

Herein, thanks to both the good chemical stability and the small number of active groups contained on the surface of h-BN, we first carried out the hydroxylation pretreatment of h-BN to enhance the reactivity. Taking it into account that the selected film-forming material contains epoxy groups, secondary functionalization with the silane coupling agent 3-glycidoxypropyltrimethoxysilane (KH560) was then conducted, which has the same epoxy group. Subsequently, BN-KH nanohybrids for corrosion protection were fabricated. Finally, epoxy resin was blended with the BN-KH nanohybrids and applied to the Q235 steel to further examine the electrochemical corrosion resistance of BN-KH/EP composite coatings. Ultimately, the results indicated that the anticorrosion performance of the composite coating with h-BN/PDA-KH560 hybrids was significantly enhanced compared with that of the other coatings.

2. EXPERIMENTAL

2.1 Materials

H-BN (~70 nm, 98%) was purchased from Bangrui Advanced Materials & Technology Co., Ltd. (Anhui, China). Absolute ethanol was provided by Sinopharm Chemical Reagent Co., Ltd. (Shanghai, China). HNO₃ (68%) and HCl (68%) were provided by Guangzhou Chemical Reagent Factor (Guangzhou, China). Xylene and n-butanol were purchased from Hubei Aosheng New Material Technology Co., Ltd. (Hubei, China) and Chinasun Specialty Products Co., Ltd. (Jiangsu, China), respectively. KH560 (3-glycidoxypropyltrimethoxysilane, 97%) was purchased from Macklin. The epoxy resin (E44) and curing agent (polyurethane 650) were provided by Zhenjiang Danbao Resin Co., Ltd. (Zhenjiang, China). The Q235 steel sheet (120×50×1.5 mm) was provided by Dongguan Tengwei Metallic Material Co., Ltd. All chemical reagents were analytically pure and were used without further purification. Deionized water was used in the experiments.

2.2 Preparation of modified BN

2.2.1 Hydroxylation of BN

The hydroxylation of BN was prepared following a previously published procedure [27]. First, 2 g of BN powder was added to 200 ml concentrated HNO₃ solution, and ultrasonically treated for 10 minutes to disperse it uniformly. Then, this suspension was magnetically stirred at 70 °C at 1440 rpm for 24 hours. The resulting suspension was centrifuged and washed with deionized water several times until the filtrate became neutral, and eventually dried at 60 °C for 24 h. The resulting materials is denoted as BN-OH and is used after being ground to a powder.

2.2.2 Silanisation of BN-OH

The details of silane grafting of hydroxylated BN by using KH560 were as follows: HCl (1 ml, 10 mol/L), was dispersed into 48 ml ethanol aqueous solution consisting of 7 ml deionized water and 41 ml ethanol, providing acidic conditions. A total of 1 wt% KH560 silane coupling agent was added dropwise, the solution was ultrasonicated for 10 min, and then magnetically stirred at 60 °C in a water bath for 3 h to fully hydrolyse the silane coupling agent. Subsequently, 0.5 g BN-OH powder was added. The mixture then was stirred at the same temperature for 3 hours and centrifuged at 12000 rpm for 10 min. The supernatant was dried in a vacuum drying oven at 90 °C for 5 hours. The modified h-BN powder, marked as the BN-KH, was centrifuged and washed with deionized water and ethanol several times before being dried at 60 °C. The obtained sample was fully ground for later use.

2.3 Preparation of Anticorrosive composite coatings

The Q235 steel sheets were polished to 1000 mesh with SiC sandpaper, washed with deionized water, and then ultrasonicated in ethanol for 10 min. After drying with cold air, the polished steel sheets were placed in a desiccator for later use.

In the coating, the content ratio of epoxy resin(E44), curing agent and the diluent was 5:5:3. The diluent was composed of 70 wt% xylene and 30% n-butanol.

First, the epoxy resin and curing agent were degassed at 60°C to increase the fluidity. BN or BN-KH powder (1 wt%) was added to the diluent and ultrasonically treated for 10 minutes to disperse it uniformly. Second, epoxy resin was added to the above-mixed solution. After the mixture was fully stirred, curing agent was added and the solution was stirred at 600 rpm for 20 minutes. Third, the solution was degassed at room temperature and low pressure and coated with a spreader on polished Q235 steel sheets. Finally, the coating was cured at room temperature for 7 days, resulting in a coating thickness of approximately 130 ± 10 μm . The pristine EP coatings were prepared in the same way with the same coating contents. The curing coatings were abbreviated as EP, BN/EP and BN-KH/EP.

2.4 Characterization Method

2.4.1 Morphological and Structural Characterizations

Prior to the measurement, the samples were fully dried in a vacuum drying oven. Fourier transformed infrared spectrometry (FT-IR, Nicolet IS50-Nicolet Continuum) and X-ray photoelectron spectroscopy (Axis Ultra DLD, England) were conducted to monitor and verify whether the BN modification treatment was successful. FTIR spectra were collected in reflection mode for the wavenumber range $4000\text{-}500$ cm^{-1} with KBr pellets as the sample matrix. The morphologies of the abovementioned composite powder and coating fracture surface were characterized by using field emission scanning electron microscopy (FESEM, Zeiss Merlin, Jena, Germany) to confirm the dispersibility of the addictive material and the defects of the coatings. In detail, the fracture surface of the coatings was obtained by breaking the cured epoxy resin in liquid nitrogen. Contact angle estimations

(Data Physics, OCA40 Micro, Stuttgart, Germany) were carried out to analyse the surface wettability of the coating.

2.4.2 Characterization of Corrosion Resistance Properties

The anticorrosion performance of the coatings was evaluated by the 3.5 wt% NaCl accelerated immersion test. All electrochemical measurements were conducted by a three-electrode system on a Princeton 263A electrochemical workstation at room temperature. The three-electrode system consisted of a saturated calomel electrode as the reference electrode, a 20 mm×20 mm platinum electrode that was used as the auxiliary electrode and a coated Q235 steel surface as the working electrode with an exposed area of 1 cm². The electrolyte was 3.5 wt% NaCl solution. The reference electrode was infinitely close to the working electrode during testing. In advance of each electrochemical measurement, the working electrode was exposed to the 3.5 wt% NaCl solution for 30 mins to obtain a stable potential. The scan range of the Tafel curve was from -500 mV~500 mV (vs. OCP) and the scan rate was 0.5 mV/s. The corrosion potential (E_{corr}) and corrosion current density (i_{corr}) were obtained by Tafel extrapolation. Furthermore, electrochemical impedance tests were recorded in the frequency range of 10⁵ to 10⁻² Hz with an AC amplitude of 20 mV. The EIS of the samples were recorded at the 0, 7, 14 and 21 days after immersion. Finally, the EIS data were fitted by ZSimpWin software to determine the change in the anticorrosion coatings during the immersion procedure.

3. RESULT AND DISCUSSION

3.1 Structures and morphologies of h-BN and modified h-BN

Figure 1 shows the FTIR spectra of pristine BN, BN-OH, and BN-KH respectively. The characteristic peaks of boron nitride appear at approximately 1380 cm⁻¹ and 800 cm⁻¹[28-30]. These are attributed to the B-N stretching vibration and B-N bending vibration, respectively. The broad band at approximately 3400 cm⁻¹ is assigned to hydroxyl groups. The hydroxyl peak of h-BN treated with HNO₃ is obviously stronger, indicating that the hydroxylation treatment of BN is successful. In addition, the vibrations of BN-OH at 1380 cm⁻¹ and 800 cm⁻¹ were also enhanced[31], which suggests that the asymmetrical vibrational dipole moments of the B-N-B and B-N bonds had become larger, arising from the absorption of some new negative functional group(-OH) on BN. The absorption peaks at 2935 cm⁻¹ and 2865 cm⁻¹ were assigned to methylene asymmetric and symmetric stretching vibrations from KH560, respectively[32-33]. The additional peaks located at 1110 cm⁻¹ come from the stretching vibration of Si-O[32]. Moreover, there is a wide range of “enhancement” from 849 cm⁻¹ to 948 cm⁻¹, which may be due to the coupling of the asymmetric stretching vibration of the epoxy group in KH560[26] with the original spectrum of h-BN. In conclusion, the peaks confirmed the presence of the silane coupling agent on the surface of BN.

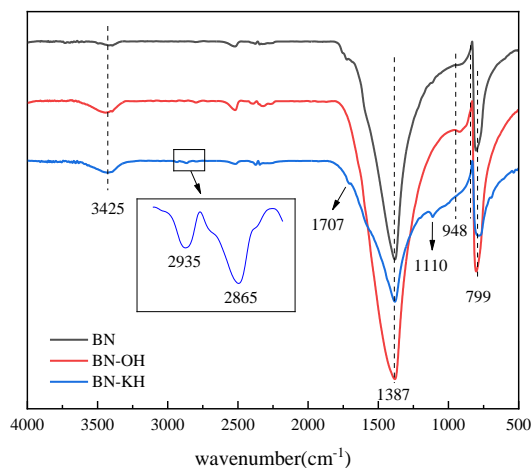


Figure 1. FTIR spectra of BN, BN-OH, BN-KH

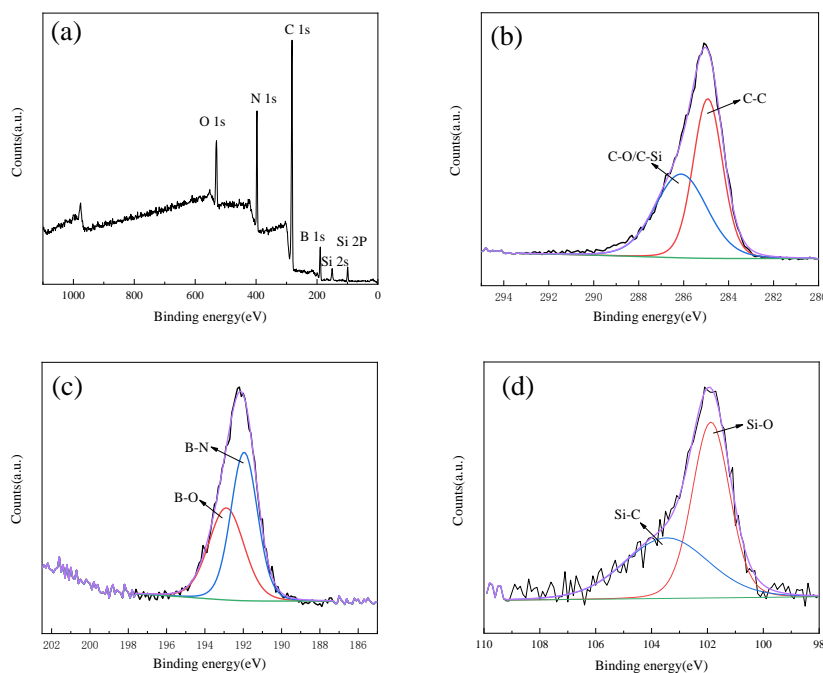


Figure 2. XPS (a) survey spectrum of BN-KH; high-resolution C 1s (b), B 1s (c) and Si 2p (d) peak-fitting curves of BN-KH

The XPS spectrum was sensitive to the surface elements and environmental substances, which can reflect the material structure and bonding details of the graft of KH560 onto h-BN. The wide scan of BN-KH powder is presented in Figure 2 (a). In addition to B and N atoms, C, O, Si atoms also appeared in the spectrum. C and O could be introduced by the air contamination. The C 1s, B 1s and Si 2p spectrum of BN-KH are demonstrated in Figure 2(b)~(d), which provides clearer evidence of chemical bonding between the BN particles and the silane curing agent[17]. The peaks appearing at 284.9 eV were considered C-C bonds (or C-H)[34], and the peaks appearing at 286.1 eV were C-O or C-Si. In B 1s spectrum, the peaks at 191.2 eV and 192.8 eV were attributed to B-N bonds and B-O

bonds[35], respectively. This indicated that the graft was connected to the B atom, which was consistent with the principle of the modification. The existence of Si confirmed the grafting of KH560. The peaks at 101.8 eV and 103.4 eV were Si-O[36] bonds and Si-C bonds, respectively. The XPS results implied that the modification was successful.

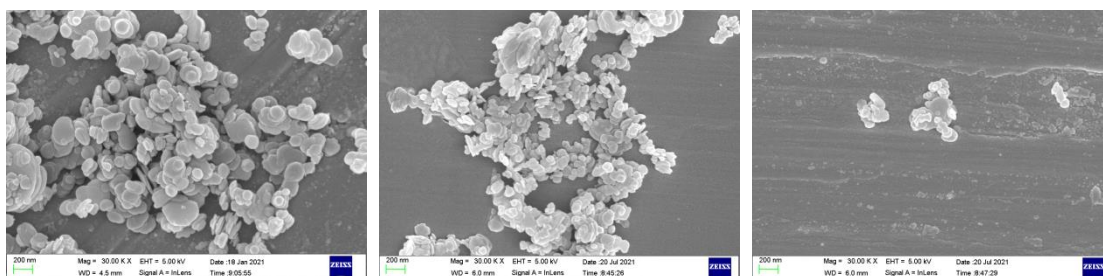


Figure 3. SEM image of (a) the pristine h-BN, (b) BN-OH, (c) BN-KH

As shown in figure 3, the pristine h-BN presented a lamellar structure with a smooth surface. Serious agglomeration occurred, which was manifested by the formation of a larger number and size of agglomerates. After the two-step modification, the agglomeration of the nanosheets was gradually ameliorated in both in size and number. The reason for the improvement in dispersion is that the siloxane deposited on the surface of h-BN prevented the h-BN sheets from reuniting into relatively large particles. The modification contributed to a great extent to the stable dispersion of the h-BN sheets in the matrix[37].

3.2 Modification principle of BN

The B-N bond of BN is partially ionic where B and N atoms are respectively electron defect and electron-rich centres, respectively. This makes it possible for the B-position to be attacked by the nucleophilic group(-OH) to acquire the hydroxylation of h-BN[38].

The focus and difficulty of the hydroxylation of BN is to activate the B atom chemically, namely, the cleavage of the B-N bond[39]. Figure 4 illustrates the two-step modification principle and steps of h-BN. The surface hydroxylation of h-BN is enhanced with oxidation by the strong acid HNO₃, thereby generating more matching of hydroxyl with B atoms at the edge surface of h-BN. Because of the large difference in polarity between the B-N and B-O bonds in the hydroxylated h-BN and the carbon chain of the organics, gaps and cracks would easily develop between the h-BN and the resin[40]. As a result, the anticorrosion performance of the BN/EP coating could not live up to expectations. It is essential to improve its compatibility with the resin for the sake of the efficient use in epoxy resin nanocomposite coatings. Hence, the subsequent modification was carried out with a silane coupling agent.

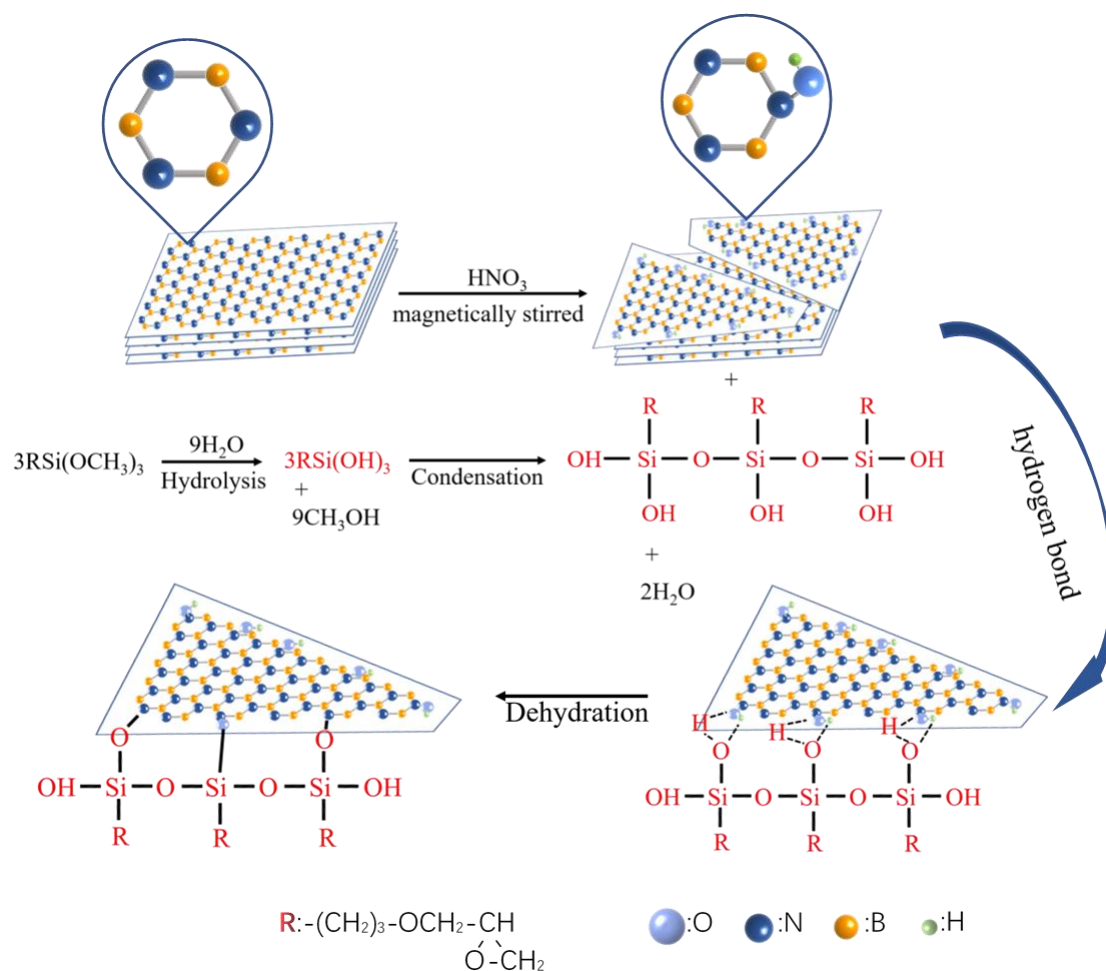


Figure 4. Reaction Methodology Folwchart

A silane coupling agent is a multifunctional molecule. One end of it reacts with the surface of the inorganic phase, while the other end selectively connects with the surrounding organic matrix phase, such as epoxy resin. The silane coupling agent has a general chemical formula $\text{R}_n\text{SiX}_{(4-n)}$ ($n < 4$, natural number)[41], where R is a nonhydrolysable group that can react with organic matter, corresponding to the epoxy group in KH560, and the X group represents a hydrolysable group, which is an indispensable group for the reaction with inorganic materials, corresponding to the methoxy group in KH560. According to the hydrolysis mechanism proposed by Pluedemann[42], the methoxy groups of the KH560 silane coupling agent are hydrolysed to the corresponding silanol in the aqueous ethanol solution with an appropriate pH. The silanol is first polymerized into oligomers, which form a hydrogen bond with the hydroxyl group at the edge of the h-BN. During the drying process [42], as the water evaporates, the oligomer turns to bonding with BN-OH by covalent bonds. Although the covalent bond was reformed during the modified procedure, the crystal configuration did not change which would not affect the chemical and physical properties of the h-BN[43]. In the end, a layer of siloxane was deposited on the surface of the h-BN Layer [27] and thus the modified h-BN can connect with the resin more closely, where the epoxy group of the deposited siloxane layer can react with the film-forming material epoxy resin to either form a chemical bond or form a physical bond such as by chelation and through van der

Waals forces. The silane coupling agent, as a bridge between two materials with different chemical properties materials, helps h-BN achieve better compatibility and dispersion in epoxy resin.

3.3 Microstructure and Morphology of Anticorrosive Coatings

To explore the effect of h-BN powder and modification treatment on the anticorrosive coatings, the fracture surfaces of EP, BN/EP, BN-KH/EP coatings were obtained after being broken by liquid nitrogen quenching. As seen in Figure 5(a)~(c), the neat epoxy resin coating showed a smooth and clean cross section with river patterns, which indicated that it has poor ductility. The fracture surface of the BN/EP coating became uneven, presenting a herringbone ridge-like pattern, and there was an interfacial slippage phenomenon on the fracture surface, which suggested that the interfacial interaction between the pristine h-BN and the epoxy resin was not intense[32]. After adding BN-KH, the flatness of the coating is obviously improved compared with that of BN/EP. The fracture surface texture has the characteristics of both EP and BN/EP, which indicates that BN-KH can connect well with the matrix due to the import of the epoxy groups in BN-KH. Then, we can conclude that BN-KH, after modification by KH560, has better compatibility with epoxy resin. Through the SEM image of the surface of the coatings(Figure 4(g)~(i)), we can intuitively find that the addition of h-BN can effectively remedy the size of the microporous defects from epoxy self-curing[41] and that the addition of BN-KH almost completely eliminated the microporous defects in the coating, demonstrating the ability of the materials with 2D lamellar structures to reduce the defects in the coatings and to promote the excellent dispersion of BN-KH.

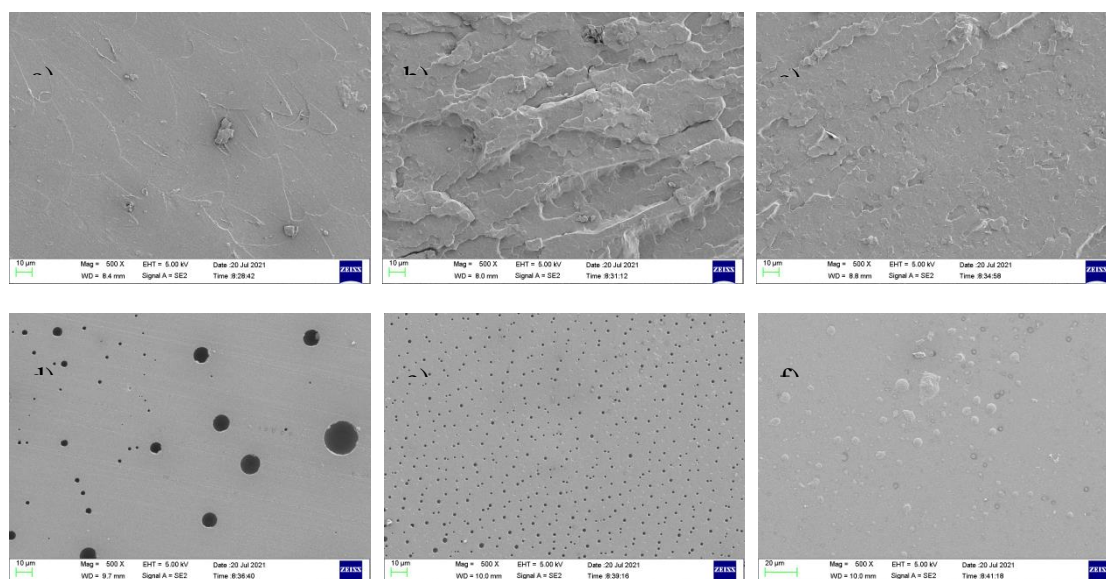


Figure 5. SEM images of the fracture surface (a)~(c) and surface morphology (d)~(f) of the nanocomposite coatings: (a)(d) EP, (b)(e) BN/EP, and (c)(f) BN-KH/EP

3.4 Evaluation of corrosion protective properties of the composite coatings

To confirm the anticorrosion properties of composite coatings, Tafel and EIS analyses were conducted.

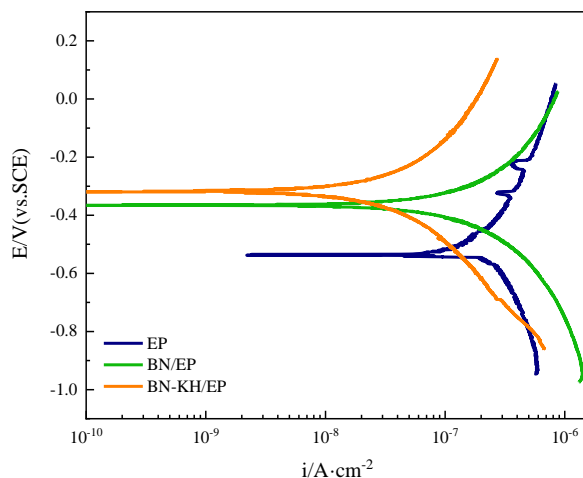


Figure 6. Polarization curves for EP, BN/EP, BN-KH/EP coating systems after 23 d of immersion in 3.5 wt% NaCl solution.

Potentiodynamic polarization curves were obtained for EP, BN/EP, BN-OH/EP coatings after 23 days of immersion in a 3.5 wt% NaCl aqueous solution at room temperature. The corrosion current (i_{corr}), corrosion potential (E_{corr}), anodic slopes (β_a), and cathodic slopes (β_c) were determined from the polarization curve using the Tafel extrapolation method. The polarization resistance (R_p) of composite coatings was obtained by the Stern-Geary equation[44]:

$$\frac{1}{R_p} = \left(\frac{\Delta i}{\Delta E} \right) E_{corr} = 2.303 \left(\frac{\beta_a + \beta_c}{\beta_a |\beta_c|} \right) i_{corr} \quad (1)$$

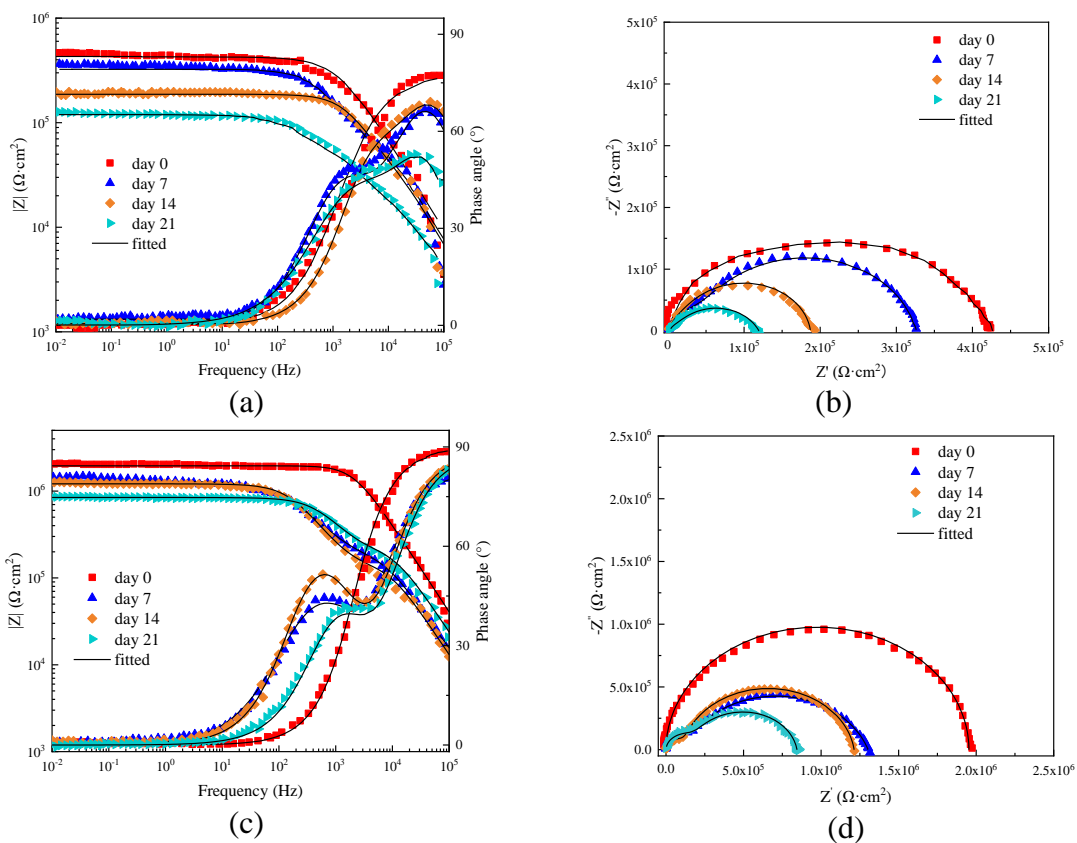
Table 1. Potentiodynamic polarization parameter values for EP, BN/EP, and BN-KH/EP coating systems after 23 d of immersion in 3.5 wt% NaCl solution

	E_{corr} (V)	i_{corr} ($A \cdot cm^{-2}$)	β_a (V/dec)	β_c (V/dec)	R_p ($\Omega \cdot cm^2$)
EP	-0.528	2.673×10^{-7}	1.117	-0.980	1.293×10^7
BN/EP	-0.367	2.441×10^{-7}	0.649	-0.607	1.641×10^7
BN-KH/EP	-0.316	5.276×10^{-8}	0.563	-0.518	5.233×10^7

The coating that has lower i_{corr} , more positive E_{corr} and higher R_p represents better anticorrosion performance. Figure 6 shows the potentiodynamic polarization curves of different coatings and the electrochemical parameters are summarized in Table 1, which reveals that these coatings vary in

corrosion-resistance properties. Compared with the epoxy resin, the polarization curve of BN/EP shifted both positively and left, corresponding to an increase in the self-corrosion potential and a decrease in the self-corrosion current of the coatings, indicating that the anticorrosion performance was improved. It can be directly calculated from the parameters in Table 1 that the self-corrosion potential of the coating with BN-KH is positively shifted by 212 mV and 51 mV, compared with EP and BN/EP, respectively. Furthermore, the corrosion current of BN-KH/EP is reduced by between half and one order of magnitude and R_p is much higher than that of the other coatings. BN-KH/EP, with the highest R_p , corrosion potential and lowest self-corrosion current[45], thermodynamically has the lowest corrosion tendency after 23 days of immersion.

Further analysis of the anticorrosion properties was conducted based on the EIS results. The Nyquist and Bode plots of EP, BN/EP, BN-KH/EP coatings immersed in 3.5 wt% NaCl aqueous solution for 0, 7, 14 and 21 days are presented in Figure 6. The diameter of the arc in the Nyquist plot intuitively indicates that there is a significant difference between these three coatings in anticorrosive performance. The larger the diameter is, the better the corrosion resistance is. As soaking time increases, the capacitive reactance arc radius gradually decreases, and the low-frequency impedance modulus continues to decrease, suggesting that the anticorrosion barrier properties of the coating were affected[46]. BN-KH/EP showed the largest diameter throughout the experimental period elucidated that the addition of BN-KH enhanced the corrosion resistance performance of EP. Furthermore, the impedance modulus $|Z|$ at the lowest frequency can reflect the barrier performance of the coating system[47].



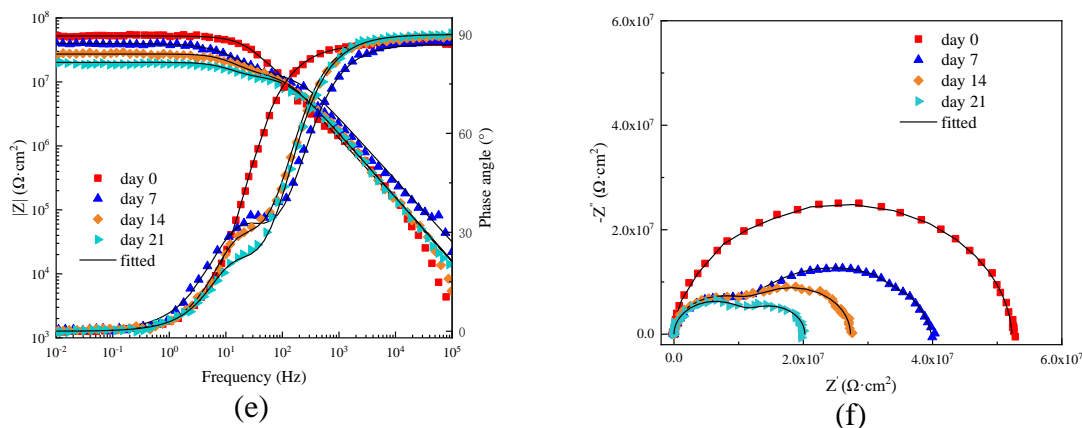


Figure 7. Nyquist and Bode plots of EP(a,b), BN/EP(c,d), BN-KH/EP(e,f) in 3.5 wt% NaCl solution after 0, 7, 14 and 21 days of immersion.

With increasing immersion time, there is a general tendency of declining $|Z|_{0.01\text{ Hz}}$ for all the coatings. The impedance values at 0.01 Hz ($|Z|_{0.01\text{ Hz}}$) of the coatings containing BN are higher than that of the blank epoxy coating during the complete stage of the immersion period. For the blank control group EP coatings, the $|Z|_{0.01\text{ Hz}}$ value dropped from $4.67 \times 10^5 \text{ } \Omega \cdot \text{cm}^2$ to $1.27 \times 10^5 \text{ } \Omega \cdot \text{cm}^2$ after 21 days. The $|Z|_{0.01\text{ Hz}}$ of BN/EP dropped from $2.05 \times 10^6 \text{ } \Omega \cdot \text{cm}^2$ to $1.44 \times 10^6 \text{ } \Omega \cdot \text{cm}^2$, $1.26 \times 10^6 \text{ } \Omega \cdot \text{cm}^2$ and $8.48 \times 10^5 \text{ } \Omega \cdot \text{cm}^2$ after 7, 14 and 21 days of immersion, respectively. The descent rate of the $|Z|_{0.01\text{ Hz}}$ first decreased and then increased, which suggested that the barrier properties of BN first played an important role in the defence against corrosive ions, as many studies in the literature reported[48-49], but the poor dispersion of BN would cause microdefects in the coating, resulting in a decrease in the corrosion resistance of the coatings. In particular, the coating with modified BN exhibited a $|Z|_{0.01\text{ Hz}}$ value reaching $5.23 \times 10^7 \text{ } \Omega \cdot \text{cm}^2$ at the preliminary stage of immersion, which was more than two orders of magnitude higher than that of the blank epoxy coating and one order of magnitude higher than that of BN/EP. Moreover, after 21 days of immersion, the $|Z|_{0.01\text{ Hz}}$ of BN-KH/EP was greater than those of EP and BN/EP by factors of 150 and 20, respectively. The $|Z|_{0.01\text{ Hz}}$ of BN-KH/EP maintained the highest values of the three kinds of coatings during the whole experimental period, indicating that BN-KH with homogeneous dispersion properties exhibited superior corrosion resistance over other coatings for the long-term period.

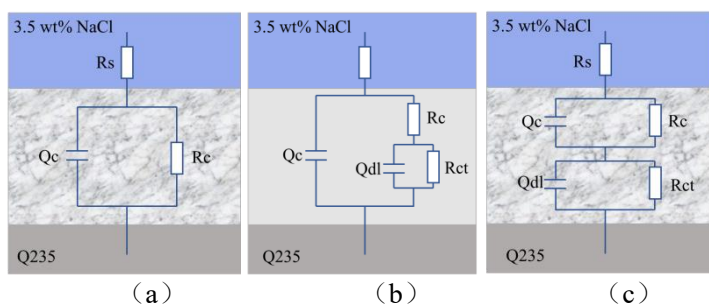


Figure 8. Equivalent electric circuit models used to fit the EIS results. (a) Initial stage of immersion for all coatings; (b) medium stage of immersion for EP; (c) medium stage of immersion for BN/EP and BN-KH/EP.

The specific corrosion process of the coating/metal system can be illustrated by the Bode phase angle. The phase angles of the EP coating were obviously lower than those of the BN/EP and BN-KH/EP coatings. As the immersion time increases, the phase angle curves of the EP coating decline considerably. The reason for this trend is that the infiltration of electrolyte solution decreased the resistance of the coatings and increased the capacitance of the EP coatings increasing. However, the phase angle of BN-KH/EP maintained a comparatively high value in the high-frequencies region (10^3 - 10^5 Hz), revealing that the BN-KH/EP layer resembled an insulating layer with a large resistance value and a small capacitance value, demonstrating better anticorrosive properties[48]. To investigate the changes in the coatings in detail, and equivalent electric circuit was used to fit the EIS data in the ZsimpWin software. According to the characteristics during different immersion periods, different impedance equivalent circuits, based on specific mechanisms, are suggested for the EP, BN/EP and BN-KH/EP coatings (Figure 8).

Generally[50], the period was defined as the initial stage of immersion before water and corrosive ions penetrated to the coating/base interface, corresponding to one time constant in the Bode phase diagram. In the initial stage of immersion, whether fillers are added will not affect the types of the components in the corresponding fitted electric circuit diagram but will affect the properties of the coating resistance, so the three fitted circuits at the initial stage of immersion are shown in Figure 8(a). When the electrolyte approaches the coating/metal interface, it will initiate a microbattery corrosion reaction. An impedance spectrum measured at this time, the so-called medium stage of immersion, will show two time constants[28]. The equivalent circuit model, shown in Figure 8(c), is chosen when the electrolyte solution penetrates to the coating system evenly. The defects, existing in BN/EP and BN-KH/EP significantly decrease compared with the EP coating both in size and number (as shown in Figure 5(d)~(f)). It is considered that the electrolyte absorbed in the coatings is evenly distributed, so the equivalent circuit of BN/EP and BN-KH/EP in the medium stage of immersion is shown in Figure 8(c). The defects that occurred on the surface of EP coatings were larger and more abundant than those on the surfaces of the other coatings; thus, it is believed that the electrolyte solution will approach the coating/metal interface from the partial coating. The equivalent circuit for EP in the medium stage of immersion is shown in Figure 8(b). It can be seen from the phase angle diagram that EP and BN/EP have two time constants after 7 days of immersion, which means that water molecules and corrosive ions are likely to have reached the interface of the metal and coatings[51], while BN-KH/EP did not exhibit the characteristic of two-time constants until 21 days of immersion, which suggests that BN-KH provides better barrier properties against the corrosive ions and significantly prevents the corrosion process of the metal substrate. The proposed equivalent circuit consists of the solution resistance (R_s), capacitance of the coating (Q_c), resistance of the coating (R_c), charge transfer resistance (R_{ct}), and electric double-layer capacitance (Q_{dl}). Q_{dl} in the equivalent circuit represents the constant phase angle element (CPE).

Table 2. Fitting electrochemical data of the EP, BN/EP, BN-KH/EP coatings in the 3.5 wt% NaCl solution

	day	R_s ($\Omega \cdot \text{cm}^2$)	Q_c ($\Omega^{-1} \cdot \text{cm}^{-2} \cdot \text{s}^n$)	n	R_c ($\Omega \cdot \text{cm}^2$)	Q_{dl} ($\Omega^{-1} \cdot \text{cm}^{-2} \cdot \text{s}^n$)	n	R_t ($\Omega \cdot \text{cm}^2$)
EP	0	3.73×10^{-6}	1.02×10^{-9}	0.87	4.26×10^5	—	—	—
	7	3.13×10^3	2.35×10^{-10}	1.00	6.50×10^4	3.691×10^{-9}	0.85	2.57×10^5
	14	2.28×10^3	2.51×10^{-10}	1.00	5.48×10^4	1.456×10^{-9}	0.87	1.30×10^5
	21	2.85×10^3	5.45×10^{-10}	1.00	1.83×10^4	2.337×10^{-8}	0.73	9.62×10^4
BN/EP	0	3.60×10^{-2}	3.92×10^{-11}	1.00	1.95×10^6	—	—	—
	7	7.93×10^{-4}	4.04×10^{-9}	0.80	1.18×10^6	1.66×10^{-9}	1.00	1.25×10^5
	14	1.00×10^{-2}	1.56×10^{-9}	0.92	1.10×10^6	1.569×10^{-10}	1.00	1.10×10^5
	21	1.00×10^{-2}	9.97×10^{-10}	0.91	6.76×10^5	8.606×10^{-11}	1.00	1.68×10^5
BN-KH/EP	0	5.66×10^{-3}	3.26×10^{-10}	0.89	5.22×10^7	—	—	—
	7	1.36×10^{-3}	2.63×10^{-10}	0.86	4.55×10^7	—	—	—
	14	5.82×10^{-3}	6.18×10^{-10}	0.80	3.02×10^7	—	—	—
	21	1.00×10^{-2}	1.16×10^{-10}	1.00	1.03×10^7	1.08×10^{-9}	1.00	8.73×10^6

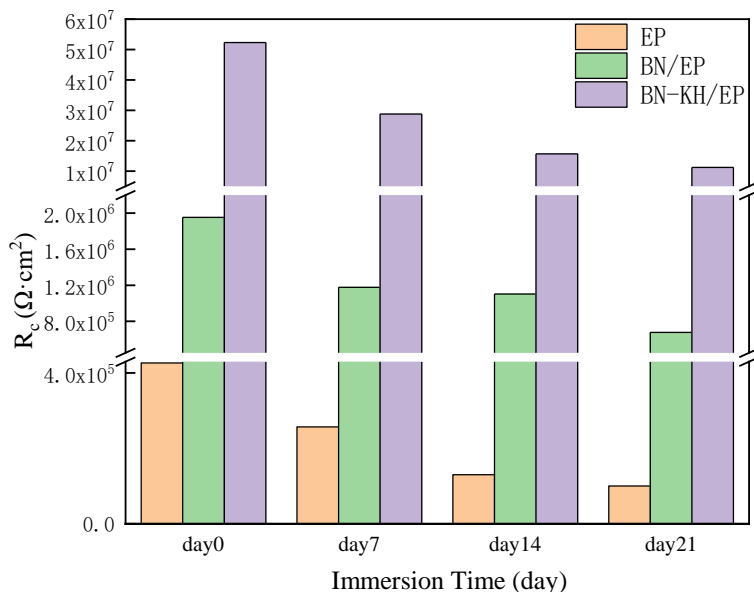


Figure 9. The fitted R_c of the EP, BN/EP, BN-KH/EP coatings

When the coating surface material is rough or unevenly distributed, the coating capacitance will deviate from the ideal behaviour, while the parameter n of Q_{dl} can properly reflect the deviation. When n is closer to 1, the element is closer to pure capacitance, and vice versa, the closer to 0, the closer to pure resistance, so it is closer to the actual situation to choose Q_{dl} instead of pure capacitive elements[52]. The fitted electrochemical data of the applied coatings immersed in the 3.5 wt% NaCl solutions are shown in Table 2, and the R_c of all the coatings is shown in Figure 9. As reported, during the initial stage of immersion, the pores and defects in the coatings would be filled with the electrolyte, decreasing the resistance values[53]. The R_c of the coating with original h-BN is dozens of times higher than that of EP, and the longer it is immersed, the more prominent the advantages it emphasizes. The R_c of the

coating with modified BN is approximately 20 times higher than that of the coating with the original h-BN, indicating that BN-KH can protect the coating from damaging corrosive ions and that BN-KH/EP can maintain an excellent anticorrosion property.

3.5 Mechanism of corrosion protection

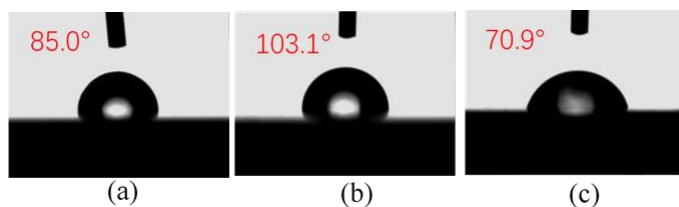


Figure 10. Contact angle images of (a)EP, (b)BN/EP, (c)BN-KH/EP

It can be seen from the electrochemical performance test that the order of the corrosion resistance properties of the three coatings from low to high is $EP < BN/EP < BN-KH/EP$. After 1% BN was added to the epoxy resin, the hydrophobicity of BN/EP increased due to the good hydrophobicity of BN, as shown in the Figure 10, which supports the anticorrosion of BN/EP coatings in the early immersion stage. After the middle immersion stage, the barrier performance of BN gradually becomes prominent, causing BN/EP to exhibit stronger anticorrosion performance than pure epoxy resin throughout the experimental period. Because of the significant polarity difference between the B-N bond in the inorganic h-BN and the carbon chain of the epoxy resin and the poor dispersion stability of the h-BN[32], gaps and cracks are likely to occur between the h-BN and the resin in the coatings, which in turn forms microporous defects and thus reduces the anticorrosion performance. After h-BN was modified by a KH560 silane coupling agent, the compatibility of h-BN and epoxy resin improved and the defects of the coating were effectively reduced, taking advantage of the “maze effect” of the two-dimensional lamellar structure of h-BN in the epoxy resin[54]. As seen from Figure 10 and Figure 5, the promotion of the anticorrosion performance of the modified BN-KH/EP coating was mainly due to the improvement in the dispersion characteristics of h-BN in the coating and the compatibility with the resin, but not because of the hydrophobicity of h-BN, which had not yet been reflected.

4. CONCLUSION

In conclusion, h-BN materials are successfully modified through a two-step treatment: first, treated with strong oxidizing acid, more hydroxyl groups attach at the edge of h-BN. Then, through the condensation reaction between silane and hydroxyl groups, the silane link is grafted onto the edge of h-BN. The introduction of epoxy groups on h-BN enhanced the connection of epoxy resin and significantly filled the microporous defects and cracks; thus, the BN-KH/EP coatings manifested good physical barrier performance against corrosive ions. The EIS results revealed that R_c is approximately one order of magnitude higher than that of the coating with the original h-BN. The self-corrosion potential of the coating with BN-KH is positively shifted by 212 mV and 51 mV compared with EP and BN/EP

respectively. Furthermore, the corrosion current of BN-KH/EP is reduced by between half and one order of magnitude and R_p is much higher than that of the other coatings. Thus, the addition of BN-KH promoted the corrosion protection of the EP coating on the Q235 steel for a long period of time.

References

1. I. Soltani, S. D. Smith and R. J. Spontak, *J. Membrane Sci.*, 526 (2017) 172.
2. R. B. Naik, S. B. Jagtap and D. Ratna, *Prog. Org. Coat.*, 87 (2015) 28.
3. M. Cui, S. Ren, S. Qin, Q. Xue, H. Zhao and L. Wang, *Corros. Sci.*, 131 (2018) 187.
4. W. Cai, N. Hong, X. Feng, W. Zeng, Y. Shi, Y. Zhang, B. Wang and Y. Hu, *Chem. Eng. J.*, 330 (2017) 309.
5. W. Jin, W. Zhang, Y. Gao, G. Liang, A. Gu and L. Yuan, *Appl. Surf. Sci.*, 270 (2013) 561.
6. T. Sainsbury, A. Satti, P. May, Z. Wang, I. McGovern, Y. K. Gun Ko and J. Coleman, *J. Am. Chem. Soc.*, 134 (2012) 18758.
7. L. Boldrin, F. Scarpa, R. Chowdhury and S. Adhikari, *Nanotechnology*, 22 (2011) 505702.
8. X. Li, P. Bandyopadhyay, T. Kshetri, N. H. Kim and J. H. Lee, *J. Mater. Chem. A.*, 6 (2018) 21501.
9. M. Cui, S. Ren, G. Zhang, S. Liu, H. Zhao, L. Wang and Q. Xue, *Journal of Chinese Society for Corrosion and Protection.*, 36 (2016) 566.
10. J. Sun, W. Cao, N. Wang, L. Gu and W. Li, *Acta Chimica Sinica.*, (2020) 1.
11. H. Liu, Z. Li, S. Wang, C. Yuan, Y. Xu, W. Luo, G. Chen, B. Zeng and L. Dai, *J. Inorg. Organomet. P.*, 30 (2020) 513.
12. Y. Bai, J. Zhang, Y. Wang, Z. Cao, L. An, B. Zhang, Y. Yu, J. Zhang and C. Wang, *ACS Appl. Nano Mater.*, 2 (2019) 3187.
13. C. Zhang, X. Hao, Y. Wu and M. Du, *Mater. Res. Bull.*, 47 (2012) 2277.
14. Y. Lin, J. W. Connell, *Nanoscale*, 4 (2012) 6908.
15. M. Schriver, W. Regan, W. J. Gannett, A. M. Zaniwski, M. F. Crommie and A. Zettl, *ACS Nano*, 7 (2013) 5763.
16. Y. Xue, X. Jin, Y. Fan, R. Tian, X. Xu, J. Li, J. Lin, J. Zhang, L. Hu and C. Tang, *Polym. Compos.*, 35 (2014) 1707.
17. K. Kim, M. Kim, Y. Hwang and J. Kim, *Ceram. Int.*, 40 (2014) 2047.
18. I. Jang, K. Shin, I. Yang, H. Kim, J. Kim, W. Kim, S. Jeon and J. Kim, *Colloids and Surfaces A: Physicochemical and Engineering Aspects*, 518 (2017) 64.
19. K. Kim, J. Kim, *Ceram. Int.*, 40 (2014) 5181.
20. J. Li, L. Gan, Y. Liu, S. Mateti, W. Lei, Y. Chen and J. Yang, *Eur. Polym. J.*, 104 (2018) 57.
21. L. Shen, Y. Zhao, Y. Wang, R. Song, Q. Yao, S. Chen and Y. Chai, *J. Mater. Chem. A.*, 4 (2016) 5044.
22. E. Husain, T. N. Narayanan, J. J. Taha-Tijerina, S. Vinod, R. Vajtai and P. M. Ajayan, *ACS Appl. Mater. Inter.*, 5 (2013) 4129.
23. J. Li, L. Gan, Y. Liu, S. Mateti, W. Lei, Y. Chen and J. Yang, *Eur. Polym. J.*, 104 (2018) 57.
24. Y. Wu, Y. He, C. Chen, F. Zhong, H. Li, J. Chen and T. Zhou, *Colloids and Surfaces A: Physicochemical and Engineering Aspects*, 587 (2020) 124337.
25. H. Huang, X. Huang, Y. Xie, Y. Tian, X. Jiang and X. Zhang, *Prog. Org. Coat.*, 130 (2019) 124.
26. C. Zhang, Y. He, Y. Zhan, L. Zhang, H. Shi and Z. Xu, *Polym. Adv. Technol.*, 28 (2017) 214.
27. A. T. Seyhan, Y. Göncü, O. Durukan, A. Akay and N. Ay, *J. Solid State Chem.*, 249 (2017) 98.
28. E. Husain, T. N. Narayanan, J. J. Taha-Tijerina, S. Vinod, R. Vajtai and P. M. Ajayan, *ACS Appl. Mater. Inter.*, 5 (2013) 4129.
29. Y. Xue, Q. Liu, G. He, K. Xu, L. Jiang, X. Hu and J. Hu, *Nanoscale Res. Lett.*, 8 (2013) 49.
30. J. Hou, G. Li, N. Yang, L. Qin, M. E. Grami, Q. Zhang, N. Wang and X. Qu, *RSC Adv.*, 4 (2014) 44282.

31. M. Du, Y. Wu and X. Hao, *Crystengcomm*, 15 (2013) 1782.
32. C. Zhang, Y. He, Y. Zhan, L. Zhang, H. Shi and Z. Xu, *Polym. Adv. Technol.*, 28 (2017) 214.
33. C. J. Kuo, G. R. S. Dewangga and J. Chen, *Text. Res. J.*, 89 (2018) 2637.
34. L. Zhao, Z. Du, X. Tai and Y. Ma, *Colloids and Surfaces A: Physicochemical and Engineering Aspects*, 623 (2021) 126404.
35. C. Y. Zhi, Y. Bando, T. Terao, C. C. Tang, H. Kuwahara and D. Golberg, *Chem. Asian J.*, 4 (2009) 1536.
36. J. Song, Z. Dai, J. Li, H. Zhao and L. Wang, *High Perform. Polym.*, 31 (2019) 116.
37. Z. Wang, Y. Fu, W. Meng and C. Zhi, *Nanoscale Res. Lett.*, 9 (2014) 643.
38. B. Zhong, J. Zou, L. An, C. Ji, X. Huang, W. Liu, Y. Yu, H. Wang, G. Wen, K. Zhao and X. Lin, *Composites Part A: Applied Science and Manufacturing*, 127 (2019) 105629.
39. Y. Lin, T. V. Williams, T. Xu, W. Cao, H. E. Elsayed-Ali and J. W. Connell, *J. Phys. Chem. C*, 115 (2011) 2679.
40. T. Zong, Y. Zhang and P. Liu, *New Chemical Materials.*, 48 (2020) 18.
41. J. Gu, Q. Zhang, J. Dang and C. Xie, *Polym. Adv. Technol.*, 23 (2012) 1025.
42. Q. Liu, J. Ding, D. E. Chambers, S. Debnath, S. L. Wunder and G. R. Baran, *J. Biomed. Mater. Res.*, 57 (2001) 384.
43. J. Yu, L. Huang, B. Kipsang and Y. Hai, *Ceram. Int.*, 47 (2021) 25551.
44. Y. Wu, Y. He, T. Zhou, C. Chen, F. Zhong, Y. Xia, P. Xie and C. Zhang, *Prog. Org. Coat.*, 142 (2020) 105541.
45. F. Xiu-qing, S. Mo-qi, L. Jin-ran, W. Xing-sheng, W. Qing-qing and X. Ye, *Int. J. Electrochem. Sci.*, 15 (2020) 816.
46. M. Guo, Q. Zeng, X. Ren, L. Xue, Y. Xin, Y. Ren, L. Xu and L. Li, *Int. J. Electrochem. Sci.*, 16 (2021) 150871.
47. W. Liu, J. Li, X. Huang and J. Bi, *Materials*, 14 (2021) 1982.
48. A. Tozar, H. Karahan, *Appl. Surf. Sci.*, 452 (2018) 322.
49. G. Chilkoor, S. P. Karanam, S. Star, N. Shrestha, R. K. Sani, V. Upadhyayula, D. Ghoshal, N. A. Koratkar, M. Meyyappan and V. Gadhamshetty, *ACS Nano*, 12 (2018) 2242.
50. C. Cao J. Zhang, *An Introduction to Electrochemical impedance spectroscopy*, Beijing, Science Press, 2002.
51. D. Xu, C. Lou, J. Huang, X. Lu, Z. Xin and C. Zhou, *Prog. Org. Coat.*, 134 (2019) 126.
52. J. Li, W. Liu and W. Xie, *Int. J. Electrochem. Sci.*, 15 (2020) 7136.
53. E. Huttunen-Saarivirta, V. E. Yudin, L. A. Myagkova and V. M. Svetlichnyi, *Prog. Org. Coat.*, 72 (2011) 269.
54. Y. Fan, H. Yang, H. Fan, Q. Liu, C. Lv, X. Zhao, M. Yang, J. Wu and X. Cao, *Materials*, 13 (2020) 2340.